Icarus 246 (2015) 237–246

Contents lists available at ScienceDirect

Icarus

journal homepage: www.elsevier.com/locate/icarus

The state of Pluto's atmosphere in 2012–2013 ☆,☆☆,☆☆☆

A.S. Bosh [a,*], M.J. Person [a], S.E. Levine [b,a], C.A. Zuluaga [a], A.M. Zangari [a,1], A.A.S. Gulbis [c,a], G.H. Schaefer [d], E.W. Dunham [b], B.A. Babcock [e], A.B. Davis [e], J.M. Pasachoff [e], P. Rojo [f], E. Servajean [f], F. Förster [g], T. Oswalt [h,2], D. Batcheldor [h], D. Bell [h], P. Bird [h], D. Fey [h], T. Fulwider [h], E. Geisert [h], D. Hastings [h], C. Keuhler [h], T. Mizusawa [h], P. Solenski [h], B. Watson [h]

[a] MIT, Department of Earth, Atmospheric, and Planetary Sciences, 77 Mass. Ave., Rm. 54-410, Cambridge, MA 02139, United States
[b] Lowell Observatory, 1400 W. Mars Hill Rd., Flagstaff, AZ 86001, United States
[c] The Southern African Large Telescope and South African Astronomical Observatory, Cape Town 0735, South Africa
[d] The CHARA Array of Georgia State University, Mount Wilson Observatory, Mount Wilson, CA 91023, United States
[e] Williams College, 33 Lab Campus Dr., Williamstown, MA 01267, United States
[f] Dept. de Astronomía, Universidad de Chile, Casilla 36-D, Santiago, Chile
[g] Center for Mathematical Modelling, Universidad de Chile, Avenida Blanco Encalada 2120, Piso 7, Santiago, Chile
[h] Department of Physics & Space Sciences and Ortega 0.8 m Telescope at the Olin Observatory, Florida Institute of Technology, 150 W. University Blvd., Melbourne, FL 32901, United States

ARTICLE INFO

Article history:
Received 24 December 2013
Revised 28 March 2014
Accepted 31 March 2014
Available online 13 April 2014

Keywords:
Pluto, atmosphere
Occultations
Atmospheres, evolution

ABSTRACT

We observed two stellar occultations on UT 4 May 2013 and UT 9 September 2012, with the aim of measuring Pluto's atmospheric parameters. Both of these events were observed by world-wide collaborations of many observers, and both occurred within 1 month of Pluto's stationary points. The PC20120909 event was observed at the McDonald Observatory (MONET 1.2-m), and Olin Observatory (the Ortega 0.8-m); the P20130504 event was observed at the Las Campanas Observatory (du Pont 2.5-m), the Cerro Tololo Inter-American Observatory (SMARTS 1-m), and the Cerro Calán National Astronomical Observatory (Goto 0.45-m). Analysis of the data indicates an atmospheric state similar to that in June 2011. The shadow radius for the event is unchanged from recent events, indicating an atmosphere that is holding stable and not in the midst of global collapse. We discuss the advantages and disadvantages of comparing various atmospheric parameters across events (the shadow radius vs. the pressure at a particular radius). These analyses suggest that Pluto will still have an atmosphere when the New Horizons spacecraft arrives in July 2015.

1. Introduction

Pluto's eccentric orbit and large obliquity result in significant changes in global and local solar insolation over the course of a Pluto year. Because its nitrogen-dominated atmosphere is supported by vapor pressure above the surface ices, the properties and existence of the atmosphere depend critically on the surface temperature of these ices. Pluto's perihelion passage was in 1989; therefore, solar insolation has been decreasing since then yet its atmosphere has persisted and even increased in pressure (Elliot et al., 2007). Pluto's atmosphere will respond to the changing insolation (Hansen and Paige, 1996; Young, 2013), and the manner in which it does is of great interest. Will the atmosphere slowly freeze out or disappear suddenly and dramatically? Models by Hansen and Paige (1996) and more recently by Young (2013) investigate the phase space of possibilities for the evolution of the atmospheric pressure, bounded by estimates of the thermal inertia of the surface ices. While recent occultation results suggest that Pluto's atmosphere may not collapse at any time during its orbit (Young, 2013; Olkin et al., 2013), other attempts at modeling

☆ Some of the data presented herein were obtained at the W.M. Keck Observatory, which is operated as a scientific partnership among the California Institute of Technology, the University of California and the National Aeronautics and Space Administration. The Observatory was made possible by the generous financial support of the W.M. Keck Foundation.

☆☆ This work is based on data obtained with the MOnitoring NEtwork of Telescopes (MONET), funded by the "Astronomie & Internet" program of the Alfried Krupp von Bohlen und Halbach Foundation, Essen, and operated by the Georg-August-Universität Göttingen, the McDonald Observatory of the University of Texas at Austin, and the South African Astronomical Observatory.

☆☆☆ Based on observations at the Olin Observatory Ortega 0.8-m telescope, which is operated by the Florida Institute of Technology.

* Corresponding author.

E-mail addresses: asbosh@mit.edu (A.S. Bosh), mjperson@mit.edu (M.J. Person), sel@lowell.edu (S.E. Levine), czuluaga@mit.edu (C.A. Zuluaga), azangari@boulder.swri.edu (A.M. Zangari), amanda@salt.ac.za (A.A.S. Gulbis), schaefer@chara-array.org (G.H. Schaefer), dunham@lowell.edu (E.W. Dunham), bryce.a.babcock@williams.edu (B.A. Babcock), allen.b.davis@williams.edu (A.B. Davis), jay.m.pasachoff@williams.edu (J.M. Pasachoff), pato@oan.cl (P. Rojo), eliseservajean@gmail.com (E. Servajean), francisco.forster@gmail.com (F. Förster), terry.oswalt@erau.edu (T. Oswalt), dbatcheldor@fit.edu (D. Batcheldor).

[1] Present address: SwRI, 1050 Walnut St., Suite 300, Boulder, CO 80303, United States.

[2] Present address: Department of Physical Sciences, Embry-Riddle Aeronautical University, Daytona Beach, FL 32114, United States.

http://dx.doi.org/10.1016/j.icarus.2014.03.048
0019-1035/

the global behavior of Pluto's atmosphere find areas within the parameter space that allow for total collapse. One of the most pressing questions is whether the New Horizons spacecraft will find an atmosphere around Pluto when it arrives at the system in July 2015. We present the results of two recent stellar occultations, in 2012 and 2013, and discuss the implications for the survival of Pluto's atmosphere through the New Horizons encounter in 2015.

2. Occultation events

In 2012 and 2013, we attempted observations of several Pluto occultations; two were successful in that the observers were within Pluto's shadow and the weather allowed observations. In Table 1, we list event parameters for our two successful events: PC20120909 and P20130504. In our naming scheme, "PC" indicates an occultation by both Pluto and Charon, while "P" indicates an occultation only by Pluto. We summarize the observing sites and detectors in Table 2.

2.1. PC20120909

The prediction for the occultation of PC20120909 (Fig. 1) placed the shadows of Pluto and Charon directly over large areas of North and South America. Although the star is only $m_R = 15$ and thus fainter than our highest SNR events, this event occurred near Pluto's stationary point. The geocentric sky-plane velocity was only 5.5 km/s rather than the more usual 20–25 km/s. As a result, this event was accessible to small telescopes down to 24 inches. Observers could employ longer than usual exposure times of up to 5 s to achieve 2 points per scale height.

As a result of the favorable viewing geometry for PC20120909, we had arranged for many observers in North and South America to observe this event. Unfortunately, weather hampered almost

Table 1
Event parameters.

	PC20120909	P20130504
Geocentric midtime (UT)	2012 September 09 02:58	2013 May 04 08:22
Earth ephemeris	DE405	
Pluto ephemeris	PLU017	
Catalog position	(J2000; epoch of event)	
Catalog	UCAC4	UCAC2
R.A.[a]	18 28 47.380 ± 0.129	18 47 52.534 ± 0.184
Dec.[a]	−19 36 36.780 ± 0.126	−19 41 24.248 ± 0.174
μ_α (mas/yr)	−4.4 ± 5.7	−5.4 ± 12.4
μ_δ (mas/yr)	−6.5 ± 5.7	−36.6 ± 12.4
Measured position	(J2000; epoch 2012.5)	
R.A.[a]	18 28 47.377 ± 0.028	18 47 52.533 ± 0.014
Dec.[a]	−19 36 36.774 ± 0.037	−19 41 24.386 ± 0.017
Geocentric close approach (arcsec)	0.044 ± 0.035	0.004 ± 0.039
Geocentric sky-plane velocity (km/s)	5.52	10.21
Magnitudes[b]		
B	16.80	13.85
V	15.86	14.13
R	15.04	14.01
J	13.04 ± 0.03	12.74 ± 0.02
H	12.23 ± 0.03	12.49 ± 0.02
K	11.99 ± 0.03	12.40 ± 0.02
Sub-occultation locations on Pluto longitude, latitude in decimal degrees	MONET I 221.5 32.7 E 296.4 −27.2 FIT I 114.8 26.2 E 43.5 −31.7	du Pont I 13.8.5 38.1 SMARTS I 130.3 39.3 E 358.5 −22.4 Santiago I 104.1 39.2 E 15.4 −10.3

[a] Positions in hms for RA, dms for Dec. Position errors (1 sigma) are in arcseconds.
[b] BVR magnitudes are from NOMAD (Zacharias et al., 2004); all are from the unpublished USNO YB6 catalog. JHK magnitudes are from 2MASS (Skrutskie et al., 2006).

Table 2
Observing sites.

	MONET	FIT	du Pont	SMARTS	Santiago
Aperture (M)	1.2	0.8	2.5	1.0	0.45
Location	McDonald Observatory, TX	Melbourne, FL	Las Campanas, Chile	Cerro Tololo, Chile	Cerro Calán, Chile
Latitude	30°40′17″	28°03′45″.46	−29°00′26″.4	−30°10′07″.92	−33°23′45″
E. longitude	−104°01′18″	−80°37′26″.8	−70°42′13″.2	−70°48′21″.83	−70°32′11″
Elevation (km)	2.0	0.006	2.325	2.2405	0.896
Detector	Apogee Alta	iKon OL936	POETS[a]	POETS[a]	POETS[a]
Filter	Clear	Open	Open	Open	Open
Exposure time (s)	5.0	5.0	0.25	1.0	1.0
Dead time (s)	3.0	1.0	0.0017	0.0017	0.0017
Series duration (UT)	2012 September 09 2:38:37–5:08:00	2012 September 09 2:24:00–3:55:30	2013 May 04 7:50:00–8:50:00	2013 May 04 6:20:00–09:50:00	2013 May 04 8:17:30–8:50:50

[a] The Portable Occultation, Eclipse, and Transit System (POETS) is described in Souza et al. (2006).

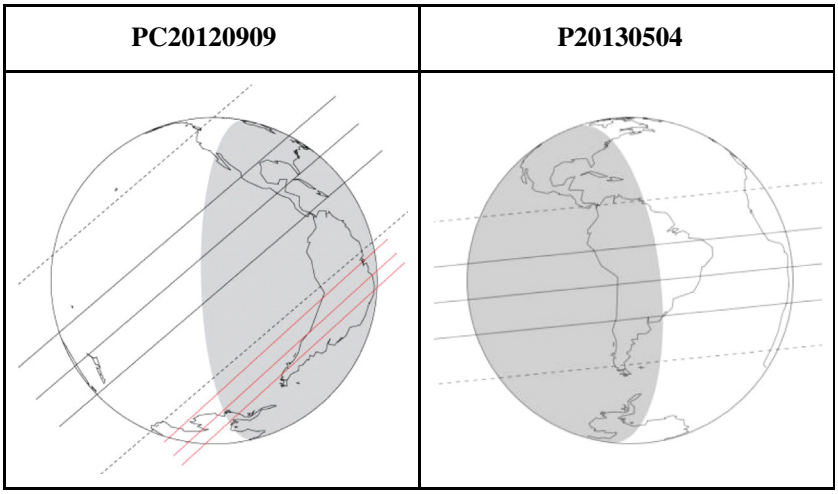

Fig. 1. Event predictions for the occultations of PC20120909 (left) and P20130504 (right) by Pluto. The thick solid lines are the prediction for the Pluto shadow (north limb, centerline, south limb). The dashed lines are the 3-sigma uncertainty from the astrometric fit. On the left panel for the PC20120909 occultation, the set of three red lines are for the Charon event that occurred approximately 40 min after the Pluto event. No error bars for the Charon event; the 3-sigma uncertainty for the Charon event is the same magnitude as that for the Pluto event. (For interpretation of the references to color in this figure legend, the reader is referred to the web version of this article.)

all observing attempts. We were successful at only two observatories: the 1.2-m MONET telescope at the McDonald Observatory and the 0.8-m Ortega telescope at the Olin Observatory at the Florida Institute of Technology.

2.1.1. PC20120909: MONET 1.2-m

Data were taken at the MONET North 1.2-m f/7 telescope at McDonald Observatory in Fort Davis, TX, but controlled remotely from MIT in Cambridge, MA. We used the facility Apogee ALTA E47 camera, which features an e2V 1024 × 1024 chip. The camera does not have frame-transfer capabilities, resulting in a dead-time of roughly 3 s between each 5 s image. The 13-μm pixels were binned 2 × 2, and a full frame was used.

The camera was chilled to −30 °C. Darks and biases were taken, and flat fields from previous observations were provided by Klaus Beuermann.

Poor weather prevented almost all preparation activities on the night before the event, save for the last 10 min of the observing session, sufficient to confirm the pointing offset to allow Pluto to be located inside in the 5.5-arcmin field of view, and acquire the separated images of Pluto and the occultation star that were later used to calculate the relative brightnesses of the two sources.

Despite a ring of clouds surrounding McDonald Observatory on the night of the observations, the sky was clear, albeit with poor seeing. The poor seeing lengthened the focusing process and delayed the start of imaging; the first image, taken at 2:38 UT coincided with immersion and observations continued until 5:08 UT.

The field of view was large enough that 4 stars were consistently available for on-chip photometry despite telescope drift.

2.1.2. PC20120909: FIT 0.8-m

The Florida Tech team observed the Pluto occultation with the Ortega 0.8-m telescope at the Olin Observatory in Melbourne, Florida. The telescope has f/8 Ritchey-Chrétien optics and an image scale of about 32 arcsec/mm. The detector was an iKon-0L936 ANDOR CCD camera with a back-illuminated E2V grade 1 CCD42-40 chip cooled to −80 °C below ambient with a five-stage Peltier cooler. Its 2048 × 2048 pixel format was binned 2 × 2 and provided a field of view about 15 arcmin square. The image acquisition system was managed by Maxim-DL controller software. The observing time base was provided by the telescope operating system to a precision of about 0.1 s.

The target field was monitored from 02:24:00 UT through 03:55:30 UT with an integration time of 5 s per frame in order to achieve a signal-to-noise of about 100. Comparison stars recommended by the MIT organizing team were used. Seeing was about 2 arcsec during the session. A cadence of about 6 s was obtained, including a read-out delay between frames of slightly less than 1 s. Data were continuously acquired during this period except for a drop-out due to a USB connector failure between 02:36 and 02:38 UT that unfortunately coincided with a portion of ingress. Nevertheless, the expected primary occultation by Pluto and its overall shape were clearly recorded.

Pluto and the occultation star images were blended and ingress had begun by 02:36:00 UT. Egress occurred at about 02:40:49 UT. The full-width-at-half-minimum of the occultation record, about 274 s, corresponded to a chord length of about 1570 km across Pluto.

2.2. P20130504

The P20130504 event (Fig. 1) was well-placed for observers in South America. Earlier predictions placed the shadow track further north, but in an unusual alignment, Pluto passed by the same star 1.5 months earlier. Due to Pluto's fortuitous path, we were able to image Pluto as it passed by the occultation star on UT 22 March 2013. Imaging with adaptive optics at the Keck Observatory showed that the occultation star was not an unresolved double star down to a limit of 50 mas; if it had been double (either physical or projected) the resulting effect on the astrometry could change the prediction by a Pluto radius or more. The appulse data also removed any uncertainty due to potential zonal errors in the astrometric network. Remaining uncertainties arise from unresolved stellar duplicity and the chosen model for Pluto's motion. The MIT group was awarded time on the Stratospheric Observatory for Infrared Astronomy (SOFIA; Becklin et al., 2007), but the southward shift of the shadow, combined with SOFIA scheduling constraints, led to a cancellation of these observations from the airborne platform. Instead, we arranged for several observers to record the event from a variety of locations in South America. The successful observations were at the du Pont 2.5 m telescope at Las Campanas Observatory, the SMARTS 1 m telescope at the Cerro Tololo Inter-American Observatory, and the 0.45 m Goto telescope at the Cerro Calán National Astronomical Observatory (OAN), in Santiago, Chile.

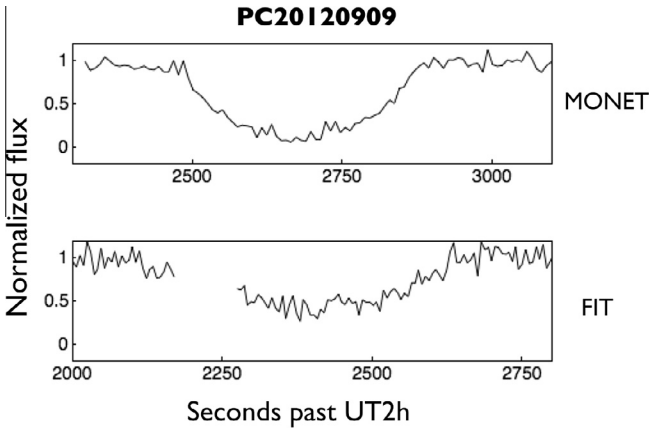

Fig. 2. Fitted sections of occultation light curves from PC20120909 event. The data dropout in the FIT data was due to a USB cable that detached briefly from the camera.

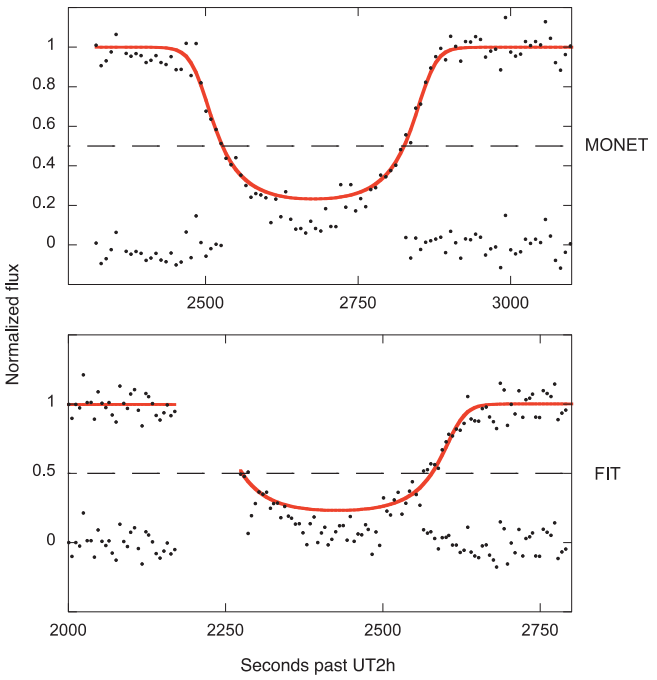

Fig. 3. Model and residuals for PC20120909 data from MONET and FIT. The model (Fit #3 in Table 3) is fit only to data between the upper baseline and the half light level (dashed horizontal line). Model residuals are plotted within each graph.

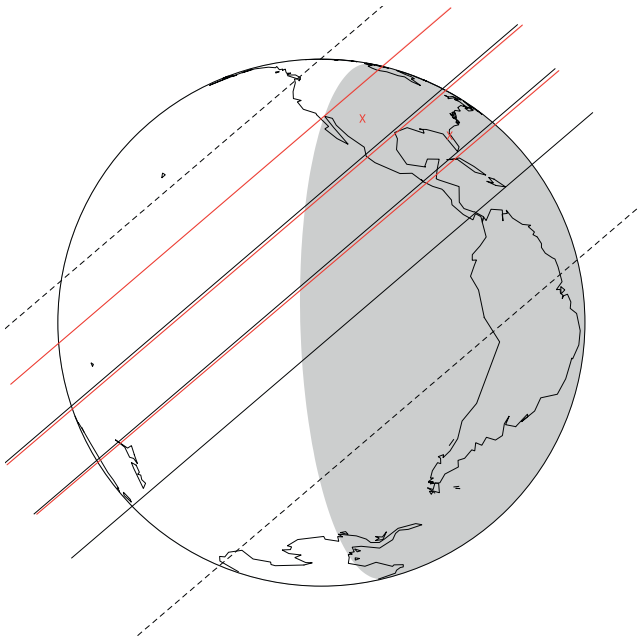

Fig. 4. Shadow path for the occultation of PC20120909 by Pluto, as determined by the geometric solution (Fit #3 in Tables 3 and 4). The geometric solution is plotted in red, while the prediction is included in black, with 3-sigma error limits (measured from north and south limbs, not from the center line). The uncertainty in the geometric positioning of the final solution (Table 4) is 24 km; error bars are not included on this plot as they are too small to be visible. For this event, which had minimal pre-event astrometric refinement, the final path moved approximately one Pluto radius to the north. The successful observing stations are indicated by red Xs: MONET in Texas and the Florida Institute of Technology. (For interpretation of the references to color in this figure legend, the reader is referred to the web version of this article.)

2.2.1. P20130504: du Pont 2.5-m

Data were gathered at the Las Campanas Observatory in Chile. The instrument used was a GPS triggered POETS system (Souza et al., 2006), mounted on the Irénée du Pont telescope 2.5-m telescope. The plate scale of the acquired data was approximately 0.35 arcsec/binned pixel (binned by 2×2); the cycle time was 250 ms. There is negligible dead time between frames in the POETS frame-transfer readout. Seeing varied from 1 arcsec down to 0.7 arcsec throughout the observations. Data were acquired before and after the event, when the star and Pluto system were well-separated, as well as during the occultation.

The resulting light curve was generated using circular aperture photometry, comparing the occultation star plus Pluto signal to 8 well-separated standard stars in the field. Analysis of the separated images taken away from the event time indicated that the occultation star yielded $48.6 \pm 0.2\%$ of the flux of the star plus Pluto images. This allowed consistent background calibration of the final du Pont light curve at a SNR of 105 per point or approximately 450 per scale height, here displayed in Fig. 4.

2.2.2. P20130504: SMARTS 1-m

We observed the Pluto occultation on the SMARTS 1 m telescope at Cerro Tololo Inter-American Observatory using a POETS occultation camera (Souza et al., 2006). The POETS system combines an Andor iXon DU-897E camera head containing a frame transfer CCD (E2V CCD-97) with a Spectrum Instruments Intelligent Reference/TM-4 GPS based triggering system.

The SMARTS 1-m telescope has a plate scale of 20.6 arcsec/mm at the f/10 Cassegrain focus. The POETS CCD has 16-μm pixels in a 512×512 array. The effective plate scale and field of view are 0.33 arcsec/pix and 2.8 arcmin, respectively.

The camera has both a conventional and an electron multiplying amplifier. We used the conventional amplifier, read out at 1 MHz in 16 bit, frame-transfer mode. The readout noise and gain for the camera were measured during a prior occultation (on 2012 October 02 UT) and were $6.7e^-$ and $1.55e^-$/ADU. Dark current was negligible since the camera head was cooled and maintained at −60 °C. The camera is capable of hardware binning, and we used both 1×1 and 2×2 binning during the two nights of observations.

We were able to use the night before the event (2013 May 03 UT) to test signal-to-noise ratios for various exposure times, and to acquire pre-event astrometric and photometric calibration data on the occultation star field. On the night of the event (2013 May 04 UT), the seeing just prior to the occultation was about 1.6 arcsec FWHM. We were able to get additional astrometric data before and after the event.

The occultation was recorded in full frame mode, binned 2 × 2 at 1 Hz cycle time for a period of 3.5 h (12,600 frames), beginning at 06:20:00 UT. All frame transfers were triggered externally by the GPS system. Pluto and the occultation star images were blended by 07:28 UT, and ingress was witnessed visually at about 08:21 UT. Egress occurred at about 08:26 UT, with the images becoming unblended by 09:27 UT.

Within the field, there are two stars brighter than the occultation star that provide good comparison stars. Because the occultation star is near the Galactic plane, finding good sky regions is a little more difficult than normal, but we were able to find two good regions to use.

2.2.3. P20130504: Santiago 0.45-m

We observed the 2013 May 04 Pluto occultation with the 0.45-m Goto telescope at the Cerro Calán National Astronomical Observatory (OAN) in Santiago, Chile, using a POETS camera cooled to −49 °C. The camera has 512 × 512 16-μm pixels. The f/12 Cassegrain system provided a plate scale of 0.61 arcsec/pixel for a field of view of 5.2 arcmin. Data were acquired with 2 × 2 binning and a 1-s cadence. A total of 2000 frames were acquired beginning at 08:17:30 UT. All frames were triggered externally by the Spectrum Instruments GPS triggering system. Skies began to clear well before 8 UT, and following some pointing difficulties, we were able to acquire Pluto and the occulted star 5 min before the event's onset. Seeing was good for Santiago, approximately 3 arcsec. Light clouds began drifting in again fairly soon after the data and dark frames were taken. Because of these cloud issues before and after the event, we were unable to take a good set of sky flats, and dome flats were not available. The field of view provided several good comparison stars for data analysis.

3. Atmosphere model fits

Pluto's atmosphere logically breaks down into two main components: what we call the upper atmosphere (generally starting approximately 3 scale heights or 150 km above the surface and continuing to the limits of occultation observability about five scale heights higher) and the lower atmosphere (everything else down to the surface). Many light curves, especially those of 1998, 2006, and 2011 (Millis et al., 1993; Elliot et al., 2006; Person et al., 2013) show a distinct discontinuity in slope at the interface between these two regions. The upper region is characterized by a smooth thermal gradient (nearly isothermal) in a clear nitrogen-dominated atmosphere (Elliot and Young, 1992). The light curve slopes in the lower region are likely caused by much steeper thermal gradients, or by extinction effects such as variable hazes; both effects require rapid temperature changes to get the ∼100 K upper atmosphere down to the surface ice temperature of approximately 40 K in just a few scale heights.

Most models treat these regions separately either implicitly or explicitly. The EY92 class of models used here (Elliot and Young, 1992) assumes the difficulties in the lower atmosphere are caused by haze which has a sudden onset point at the slope discontinuity. Above this point, the model assumes nothing more than the behavior of refractive ideal gases. For the lower atmosphere, this exponential haze model fits the 1988 data quite well but has more difficulties with the 2011 data, or more specifically, with any light curve that includes a central flash as it tends to be eliminated by the modeled hazes in the lower atmosphere. Others (Stansberry et al., 1994; Hubbard et al., 1990) have proposed strong thermal gradients as an alternative explanation. Both the rapidly changing refraction due to these gradients and the extinction due to hazes are plausible explanations for the light curve behaviors and thus indistinguishable for this kind of occultation data. Indeed, given that there are strong observational indications of haze some years (e.g. 2002, (Elliot et al., 2003)) and not in others (e.g. 2011, (Person et al., 2013)), a varying combination of these two effects is likely responsible. Given the difficulties of distinguishing these two effects, it is reasonable to focus current analytic modeling efforts on the upper atmosphere until a deep occultation with a full spectral data set becomes available. While the largest changes in Pluto's atmosphere are likely occurring in the lower region, their effects should be seen in the upper atmosphere as varying pressures at particular altitudes or half-light radii.

The selection of a data cutoff point (Zangari, 2013) is therefore critical to the atmospheric modeling. If the data are cut too low, the upper atmospheric model will be contaminated with lower atmospheric effects. All light curves that show a clear slope discontinuity place it at or below the half-light level. We thus perform our analyses utilizing only data above the 50% flux level. These data, when interpreted using a consistent model or set of models, should result in the most directly comparable set of atmospheric parameters across a number of data sets, with the fewest number of complicating assumptions, keeping analyses as close to the actual observables as possible.

For the atmosphere fits, we used a model derived from Elliot and Young (1992), as described in Person et al. (2013). The atmospheric parameters include r_h, the half-light radius in Pluto's atmosphere, the thermal gradient parameter b, and the ratio of gravitational to thermal energy λ (Elliot et al., 2007). The thermal structure is described as $T(r) = T_h(r/r_h)^b$ where $T(r)$ is the temperature as a function of radius r from the center of Pluto, T_h is the temperature at the reference half-light point. For an isothermal atmosphere, $b = 0$. The parameter λ is also described as the atmospheric binding parameter and is used to calculate the atmospheric pressure as a function of radius. One of the most directly measured atmospheric parameters is the shadow radius at half light (referred to as the "shadow radius"). As the name implies, this is the radius as observed within Pluto's shadow of the half-light point of the light curve. For an isothermal atmosphere, this radius is smaller than the half-light radius in the atmosphere by one scale height. The important feature of this parameter is that it is independent of atmospheric model.

We fit each occultation event separately, in sets of two light curves for PC20120909 and three light curves for P20130504. We included data only from the upper atmosphere (down to the half-light level) in order to avoid the complexities of the lower atmosphere, with the various potential models employed to describe the deviations from an isothermal atmosphere. Each light curve was weighted within the fit according to its overall signal-to-noise ratio. We allowed for an offset between the star position and Pluto's ephemeris (f_0, g_0), as well as overall light curve scaling for those datasets for which we were not able to obtain separated photometry in order to normalize the light curves: FIT (PC20120909) and Santiago (P20130504). All stations employed accurate time signals, therefore no time offsets were allowed as free parameters. For each event, we perform a suite of fits that tests the sensitivity of the data to the effects of the atmospheric parameters of the half-light radius, the atmospheric binding parameter (λ), and the thermal gradient parameter (b). We begin by fitting with these parameters held fixed at recent values (from Person et al., 2013), and then proceed to free each parameter in turn, if warranted by the data. Fit results are summarized in Table 3 and are discussed below by event. We include reference fits from the PC20110623 event (Person et al., 2013) for comparison.

3.1. PC20120909

In Table 3, we present the result of the fits to the PC20120909 data. Fit #1 fixes the atmosphere parameters at their average

Table 3
Pluto atmosphere model fits.

	Reference atmosphere: PC20110623			PC20120909			P20130504			
	Ref. fit A	Ref. fit B	Ref. fit C	Fit #1	Fit #2	Fit #3[b]	Fit #4	Fit #5	Fit #6	Fit #7[b]
χ^2 per degree of freedom	1.14	1.14	1.11	1.01	1.01	1.01	1.54	1.24	1.23	1.22
Shadow radius (km)	1207.3 ± 0.1	1206.5 ± 1.0	1156 ± 17	1207.3 ± 0.1	1200 ± 11	1191 ± 29	1207.3 ± 0.1	1239.1 ± 2.8	1212.8 ± 4.3	1188.7 ± 7.7
H_P (km)	54.3 ± 0.1	54.2 ± 0.1	61.2 ± 1.0	54.2 ± 0.1	53.9 ± 0.5	56.7 ± 7.6	54.3 ± 0.1	55.7 + 0.1	57.4 ± 0.3	54.4 ± 0.5
P_h (μbar)	1.52 ± 0.01	1.52 ± 0.01	2.39 ± 0.12	1.48 ± 0.01	1.48 ± 0.01	1.72 ± 0.68	1.48 ± 0.01	1.48 ± 0.01	1.70 ± 0.03	1.66 ± 0.03
T_h (K)	95.5 ± 0.1	95.5 ± 0.1	110.7 ± 1.7	95.5 ± 0.1	96.0 ± 0.1	101 ± 15	95.5 ± 0.1	93.0 ± 0.2	99.1 ± 0.9	94.6 ± 1.0
dt/dr (K/km)	−0.16 ± 0.01	−0.16 ± 0.01	−0.24 ± 0.03	−0.16 ± 0.01	−0.16 ± 0.01	−0.17 ± 0.03	−0.16 ± 0.01	−0.15 ± 0.01	−0.17 ± 0.01	−0.24 ± 0.01
r_h (km)	1291.1	1290.3 ± 1.1	1273.1 ± 4.0	1291.1	1284 ± 12	1282 ± 14	1291.1	1325.1 ± 3.0	1304.0 ± 3.8	1299.2 ± 3.8
λ_h	18.3	18.3	14.0 ± 0.9	18.3	18.3	17.1 ± 3.1	18.3	18.3	17.2 ± 0.2	15.6 ± 0.3
b	−2.2	−2.2	−2.7 ± 0.4	−2.2	−2.2	−2.2	−2.2	−2.2	−2.2	−3.3 ± 0.2
f_0 (km)	–	–	–	−5252 ± 12	−5253 ± 12	−5253 ± 12	−2545.6 ± 0.5	−2608.7 ± 1.1	−2601.7 ± 1.5	−2601.5 ± 1.5
g_0 (km)	–	–	–	5140 ± 17	5148 ± 20	5147 ± 21	2283.1 ± 2.3	2930 ± 11	2859 ± 15	2856 ± 14
Time of half light at ingress[a]	–	–	–	2:42:04	2:42:06	2:42:08	8:21:27	8:21:28	8:21:28	8:21:29
(f, g) of half light at ingress				(−1215, 131)	(−1208, 128)	(−1201, 135)	(−1214, 142)	(−1148, −505)	(−1151, −433)	(−1145, −430)

[a] UT time of model half-light point on date of occultation.
[b] Adopted solution.

Table 4
PC20120909 impact parameters (km).

	Fit #1	Fit #2	Fit #3
MONET	851	846	844
FIT	−833	−837	−839
Uncertainty	17	22	24

values, Fit #2 adds the half-light radius (r_h) to the fitted parameters, while Fit #3 allows both half-light radius and atmospheric binding parameter (λ) to be free parameters. We also attempted a fit in which the thermal gradient parameter (b) is a free parameter, but the data were not of sufficient signal-to-noise ratio to constrain this parameter. In Table 4, we present the fitted geometric impact parameters for each station, in each model. A negative impact parameter indicates a station that is south of the occultation shadow center line. The best fit solution, Fit #3 in Table 3, is plotted in Fig. 3.

The MONET schedule allowed for imaging of the Pluto/star pair the first night, when they were well separated. This was not possible at FIT. Therefore, the MONET light curve is calibrated for absolute levels, while the FIT light curve is not (Fig. 2). We tested the sensitivity of the atmosphere parameters to the uncertainties in the light curve scaling by adding a scaling fit parameter (called background fraction after Elliot et al. (2007)). In practice, this scaling parameter was not well-constrained and wandered by much more than the formal fitted uncertainty while having little effect on the atmospheric parameters. Therefore, we fixed the background fraction at a value consistent with that used for the MONET data. Although not strictly accurate due to the different wavelength response of the data system, fits had shown that the exact value was not critical.

Figs. 4 and 5 show the geometric solution (Fit #3 from Table 3): Fig. 4 shows the shadow paths on the Earth as seen from Pluto, and Fig. 5 shows the apparent path of the star behind Pluto as seen from the observing stations. In Figs. 5 and 9, the visible pole is Pluto's north pole (positive pole for prograde rotation).

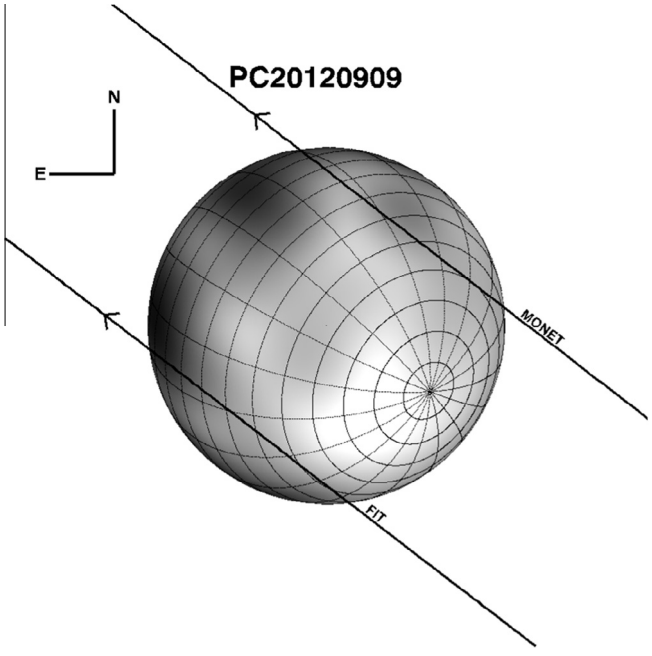

Fig. 5. Apparent paths of the occultation star PC20120909 behind Pluto, as seen from observing stations MONET and FIT. The Pluto globe shows albedo shading from Buie et al. (2010). Pluto's north (positive) rotational pole is seen in this view.

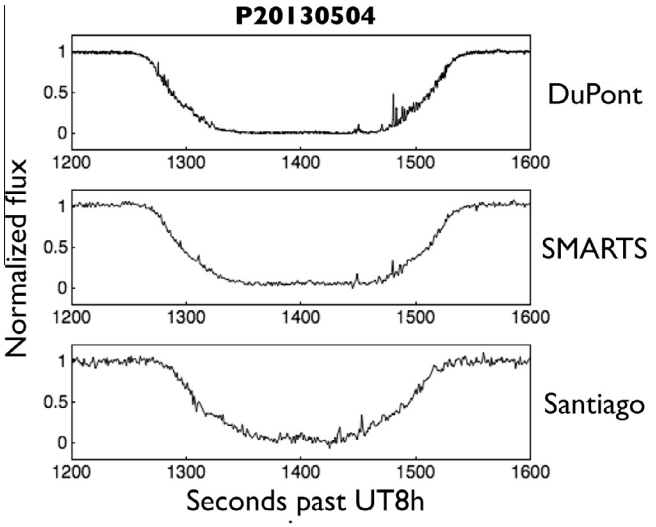

Fig. 6. Fitted sections of occultation light curves from P20130504 event, plotted at full time resolution.

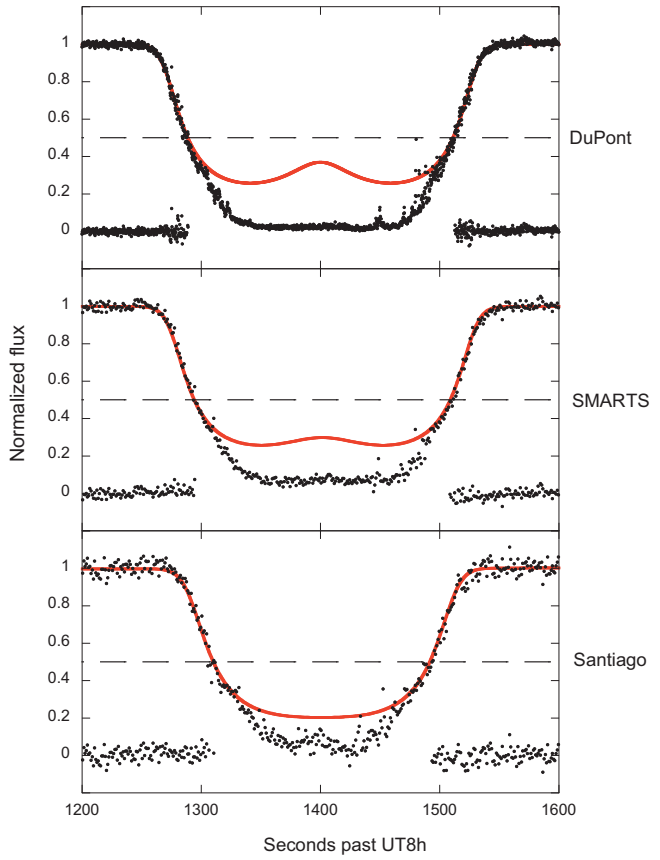

Fig. 7. Model and residuals from du Pont, SMARTS, and Santiago. The model (Fit #7 in Table 3) is fit only to data between the upper baseline and the half light level (dashed horizontal line). Model residuals are plotted within each graph.

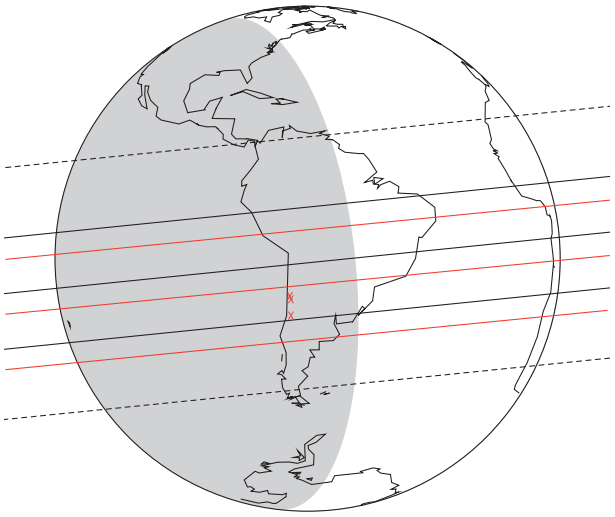

Fig. 8. Shadow path for the occultation of P20130504 by Pluto, as determined by the geometric solution (Fit #7 in Tables 3 and 5). The geometric solution is plotted in red, while the prediction is included in black, with 3-sigma error limits (measured from north and south limbs, not from the center line). The uncertainty in the geometric positioning of the final solution (Table 5) is 15 km; error bars are not included on this plot as they are too small to be seen. This event had more pre-event astrometry than did PC20120909; the remaining 3-sigma prediction uncertainty is smaller than for PC20120909 and is due to the uncertainty in the Pluto ephemeris correction model (Person et al., in preparation). From our data, we determine that the shadow shifted to the south by 550 km; this is less than the 1-sigma uncertainty of the prediction. The successful observing stations are indicated by red Xs: the du Pont and SMARTS symbols are almost on top of each other, with the Santiago symbol further to the south. (For interpretation of the references to color in this figure legend, the reader is referred to the web version of this article.)

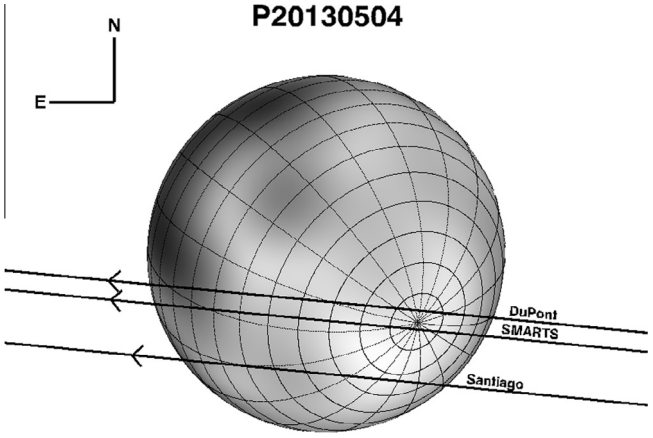

Fig. 9. Apparent paths of the occultation star P20130504 behind Pluto, as seen from observing stations du Pont, SMARTS, and FIT. The Pluto globe shows albedo shading from Buie et al. (2010). Pluto's north (positive) rotational pole is seen in this view.

3.2. P20130504

Several general features of the P20130504 light curves (Fig. 6) are worthy of note. The light curves are bowl-shaped, without the sharp drop seen in the 1988 Pluto occultation (Elliot et al., 1989). This bowl shape is seen in recent occultation profiles, notably 2011 (Person et al., 2013). Additionally, there is a set of light-curve spikes on emersion, generally attributed to small-scale temperature inversions in the atmosphere. These spikes are seen most clearly in the du Pont data, as that data set has the highest temporal resolution. However, they are clearly visible (and with similar structure) in the SMARTS data as well. The Santiago data also shows hints of these features. While interesting for the clues these provide regarding the stability of the lower atmosphere, we will not address these features further in this work, because here we confine ourselves to the upper atmosphere.

Of these light curves, the data from both du Pont and SMARTS were able to be photometrically calibrated with pre- or post-occultation resolved imaging of the star and Pluto. Due to weather issues, this was not possible at Santiago, therefore that light curve is approximately normalized and the background fraction parameter is utilized to correct for this approximation. In Table 3, we present the atmospheric fit results. Similar to the fits for the data from the PC20120909 event, we restrict the data used to that above half-light in order to avoid issues in the lower atmosphere; in this case, those issues include the light curve spikes. The first fit (#4) is performed with the atmospheric parameters of half-light radius, atmospheric binding parameter (λ) and thermal gradient parameter (b) fixed at the values found in 2011 (Person et al., 2013). We include the half-light radius (Fit #5), the atmospheric binding parameter (Fit #6), and finally add the thermal gradient parameter (Fit #6) as fitted parameters. Notice that the shadow radius is unchanged from 2012 (compare Fits #3 and #7 in Table 3), as is expected due to the short time between the two events as well as the similarities between the light curves. Table 5 lists the impact parameters of the observing stations for each of the fits. While Fit #4, the fit that is most artificially constrained, suggests that the three stations straddle the centerline, the better fitting results (Fits #5–7) place all three stations to the south of the centerline. As a result, the geometric constraint on these data fits is not as strong as it would have been if we had had stations north of Pluto's centerline. This is reflected in the relatively larger error bars on the impact parameters and the atmospheric parameters, when compared with similar results from an event such as PC20110623

Table 5
Close approach distances (km).

	Fit #4	Fit #5	Fit #6	Fit #7
du Pont	259	−391	−320	−317
SMARTS	133	−517	−446	−443
Santiago	−218	−868	−797	−794
Uncertainty	2	11	15	15

(Person et al., 2013). The model and residuals for our adopted solution (Fit #7 in Table 3) are plotted in Fig. 7. Figs. 8 and 9 give the geometric solution (Fit #7 from Table 3). Figs. 8 shows the shadow paths on the Earth as seen from Pluto, and Fig. 9 shows the apparent path of the star behind Pluto as seen from the observing stations.

4. Discussion

There are several methods in the current literature for comparing Pluto atmosphere parameters that are derived from different occultation events. There is an intrinsic difference among these occultations, in that each samples a different region on Pluto. While there have been hints at non-uniformity in previous data sets (Zangari, 2013) and models to suggest that heterogeneity may increase with decreasing temperatures on Pluto (Michaels, 2013), to date there is no strong signature of heterogeneity in the occultation light curves. If we assume atmospheric uniformity, then interpretation of the light-curve fits hinges on our choice of what to compare. One choice has been the shadow radius of the occultation, as this is a quantity that is directly determined from the occultation data with minimal modeling. This has been the choice for Elliot et al. (2007) and Person et al. (2008, 2013). Values of the half-light shadow radius are listed in Table 6.

While the half-light shadow radius is a direct measure of the state of Pluto's atmosphere along the line-of-sight of the occultation, it has been noted via atmospheric modeling that similar half-light shadow radii can be observed for decidedly different atmospheric structures (Zalucha and Gulbis, 2012). The modeled pressure changes in Pluto's atmosphere suggest that an investigation is warranted into the pressure changes in Pluto's atmosphere over time. Thus we calculate the pressure at a radius of 1275 km (chosen to facilitate comparison with others); these values are listed in Table 6. It bears keeping in mind that these pressure values are highly model dependent.

In Fig. 10, we plot the shadow radius and pressure at 1275 km as a function of time, and compare them to the models of Hansen and Paige (1996). The Hansen & Paige models present a variety of scenarios, based on a range of thermal inertia values for the surface ices. For ease of comparison, we have converted the pressure levels given by Hansen & Paige into shadow radii for Fig. 10a. Note that the range of observations plotted, either in shadow radius or in pressure, cover the range of Hansen & Paige

Table 6
Pluto atmosphere parameters for comparison across events.

Event date (UT)	Shadow radius (km)	P at 1275 km (μbar)	References
2013 May 4	1213 ± 4	2.8 ± 0.3	This work
2012 September 9	1194 ± 38	2.0 ± 2.0	This work
2011 June 23	1205 ± 2	2.0 ± 0.1	Person et al. (2013)
2007 March 18	1207 ± 4	2.0 ± 0.3	Person et al. (2008)
2006 June 12	1208 ± 4	1.6 ± 0.6	Elliot et al. (2007)
2002 August 21	1218 ± 6	1.8 ± 1.0	Elliot et al. (2007)
1988 June 9	1168 ± 10	1.0 ± 0.7	Elliot et al. (2007)

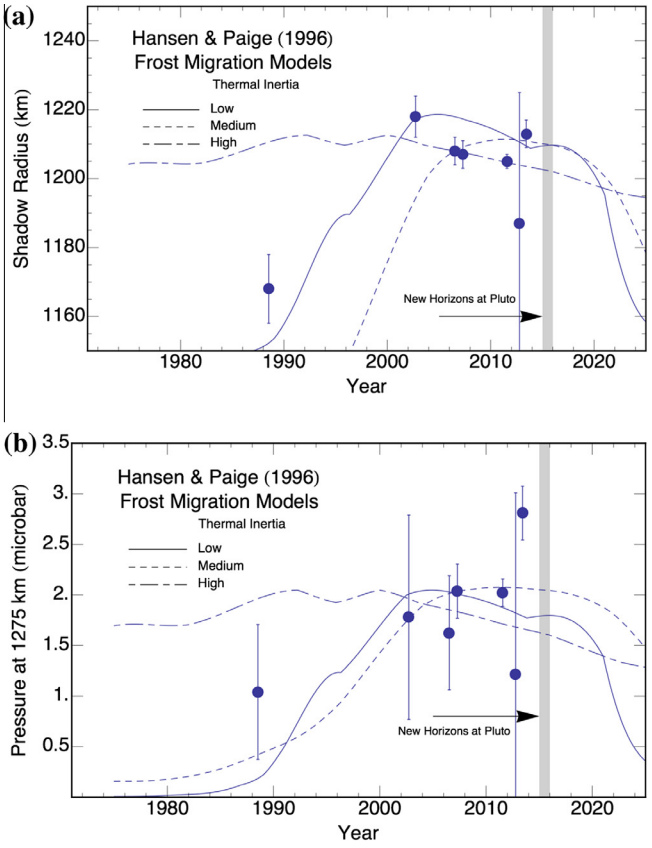

Fig. 10. Measurements of the extent of Pluto's atmosphere, as determined via several stellar occultations between 1988 and 2013. The frost migration model predictions of Hansen and Paige (1996) are also included, to provide context for the differing measurements. The arrival time of the New Horizons spacecraft at Pluto is indicated by the grey vertical bar. (a) Shadow radius vs. year. (b) Atmospheric pressure at a radius of 1275 km vs. year.

models, but due to relatively large error bars, they do not favor any one model. In pressure, the latest occultation measurement in 2013 implies a further increase of the pressure, similar in scope to the pressure increase between 1988 and 2002.

More recent work by Young (2013) presents models for the evolution of Pluto's atmosphere over its orbital period. They consider thermal inertia, volatile inventory, and volatile exchange to develop a group of potential models for the future of Pluto's atmosphere. This work is expanded upon by Olkin et al. (2015), who compare the pressure levels of various models with the recent occultation data, including separate data from the P20130504 event. For this event, they find a similar pressure increase as we find in our models (Tables 3 and 6). However, one difficulty of comparing the pressure in Pluto's atmosphere is the dependence on the model used in order to extract that pressure value. For instance, in Fig. 10b and Table 6, we see the increase in pressure between 2011 and 2013 was 2.02 ± 0.14 to 2.81 ± 0.27 μbar. This is a statistically significant difference in temperature, yet other parameters in the atmosphere model were also changing; these are summarized in Table 3. In Fig. 11, we see occultation data from 2011 to 2013 plotted together. For these data sets, only the data above half-light were used in the fit. As is evident from these data, over that range the two data sets are almost indistinguishable, yet their atmospheric fits result in different pressures. Here, the shadow radius is a more robust parameter for comparison; the difference in shadow radius for these two data sets is 26 ± 38 km.

The higher signal-to-noise ratio light curves are included in Fig. 12. The differences and similarities in these light curves are

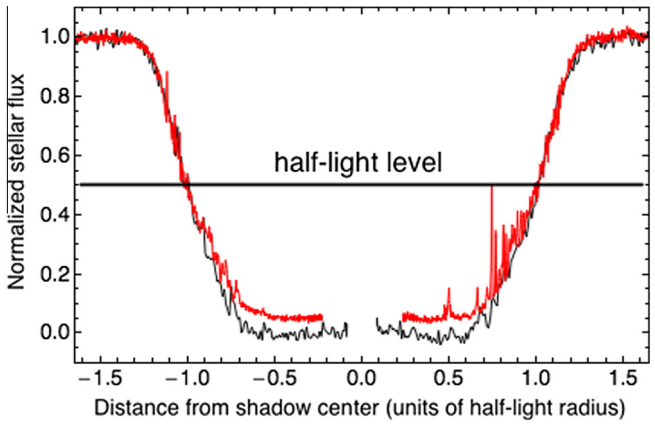

Fig. 11. Light curves from PC20110623 (black) and P20130504 (red), plotted on a common scale. The light curve segments above 0.5 light level are used in the atmospheric fits; at these levels, the curves are almost indistinguishable yet result in different fitted pressures. (For interpretation of the references to color in this figure legend, the reader is referred to the web version of this article.)

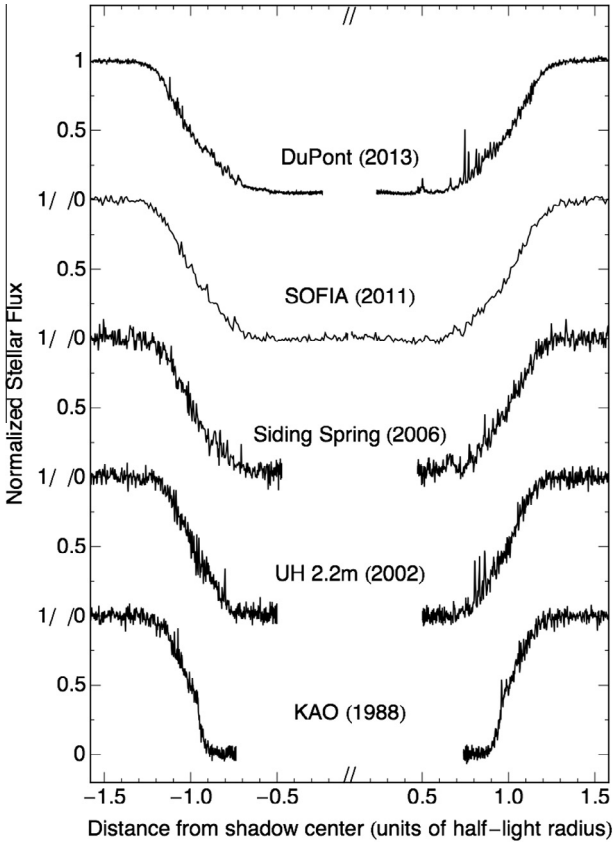

Fig. 12. Five occultation light curves from 1988 to 2013, plotted on a common scale. Note the similarities in the curves from 2002 to 2013. The 1988 light curve stands out as significantly different from the others due to its change in slope (the "knee") in the lower atmosphere.

striking, and are discussed in detail in Person et al. (this issue). Here we note a substantial difference in the upper atmosphere light curve of the 1988 data, when compared with the other data. This is best reflected in the values for the shadow radius, which shows one value for 1988 and a set of very similar values for the 2002–2013 data.

Recalling the discussion in Section 4, we prefer to use shadow radius as our direct proxy for the "size" of Pluto's atmosphere as it requires the fewest assumptions about the lower atmospheric state and upper atmospheric temperature structure. Using this proxy we find that the atmosphere has not continued to grow through 2013 as might be interpreted from the model-dependent pressure measurements. Regardless of which parameter is chosen to represent the overall state of Pluto's atmosphere however, it is clear that the atmosphere persisted through 2013 and its eventual collapse (if any) has not yet begun. Further, the current 2013 measurements of Pluto's atmosphere suggest that Pluto will have an atmosphere when New Horizons arrives at Pluto in 2015, as there is no current model that predicts a collapse so sudden that the atmosphere will freeze out within two years.

Acknowledgments

We are grateful to Steve Heathcote (SOAR director), for making arrangements for us to use the SMARTS 1.0-m telescope, after we were unable to use SOAR due to technical troubles with the telescope. We would like to thank the members of the SOAR and CTIO staff for helping us to shift telescopes at the last moment and for making our observations go smoothly.

We thank Klaus Beuermann and Frederic Hessman for ongoing MONET support.

This work was supported in part by NASA Planetary Astronomy Grants to MIT (NNX10AB27G) and Williams College (NNX08AO50G, NNH11ZDA001N), as well as Grants from USRA (#8500-98-003) and Ames Research (#NAS2-97-01) to Lowell Observatory.

A.S.B. was supported by a NASA Keck PI Data Award, administered by the NASA Exoplanet Science Institute. Data presented herein were obtained at the W.M. Keck Observatory from telescope time allocated to the National Aeronautics and Space Administration through the agency's scientific partnership with the California Institute of Technology and the University of California. The Observatory was made possible by the generous financial support of the W.M. Keck Foundation.

Observations made at FIT were partially supported by the James and Sara Ortega Endowment.

P.R. acknowledges support from FONDECYT through Grant 1120299.

F.F. acknowledges support from FONDECYT through Grant 3110042 and support provided by the Millennium Center for Supernova Science through Grant P10-064-F, funded by "Programa Bicentenario de Ciencia y Tecnología de CONICYT" and "Programa Iniciativa Científica Milenio de MIDEPLAN".

E.S. acknowledges partial support from Programa Nacional de Becas de Postgrado (CONICYT Grant 21110496).

References

Becklin, E.E., Tielens, A.G.G.M., Gehrz, R.D., Callis, H.H.S., 2007. Stratospheric Observatory for Infrared Astronomy (SOFIA). Proc. SPIE 6678, 66780A-1–66780A-8.

Buie, M.W., Grundy, W.M., Young, E.F., Young, L.A., Stern, S.A., 2010. Pluto and Charon with the Hubble Space Telescope. II. Resolving changes on Pluto's surface and a map for Charon. Astron. J. 139, 1128–1143.

Elliot, J.L., Young, L.A., 1992. Analysis of stellar occultation data for planetary atmospheres. I. Model fitting, with application to Pluto. Astron. J. 103, 991–1015.

Elliot, J.L., Dunham, E.W., Bosh, A.S., Slivan, S.M., Young, L.A., Wasserman, L.H., Millis, R.L., 1989. Pluto's atmosphere. Icarus 77, 148–170.

Elliot, J.L., Ates, A., Babcock, B.A., et al., 2003. The recent expansion of Pluto's atmosphere. Nature 424, 165–168.

Elliot, J.L., Person, M.J., Gulbis, A.A.S., et al., 2006. The size of Pluto's atmosphere as revealed by the 2006 June 12 occultation. Bull. Am. Astron. Soc. 38, 541.

Elliot, J.L. et al., 2007. Changes in Pluto's atmosphere: 1988–2006. Astron. J. 134, 1–13.

Hansen, C.J., Paige, D.A., 1996. Seasonal nitrogen cycles on Pluto. Icarus 120, 247–265.

Hubbard, W.B., Yelle, R.V., Lunine, J.I., 1990. Nonisothermal Pluto atmosphere models. Icarus 84, 1–11.

Michaels, T.I. 2013. Pluto: Global modeling of 3-D atmosphere–surface interactions. In: DPS #45 Abstract #310.02.
Millis, R.L., Wasserman, L.H., Franz, O.G., et al., 1993. Pluto's radius and atmosphere: Results from the entire 9 June 1988 occultation data set. Icarus 105, 282–297.
Olkin, C.B. et al., 2013. The May 4, 2013 stellar occultation by Pluto and implications for Pluto's atmosphere. In: DPS #45 Abstract #404.02.
Olkin, C.B. et al., 2015. Pluto's atmosphere does not collapse. Icarus 246, 220–225.
Person, M.J. et al., 2008. Waves in Pluto's upper atmosphere. Astron. J. 136, 1510–1518.
Person, M.J. et al., 2013. The 2011 June 23 stellar occultation by Pluto: Airborne and ground observations. Astron. J. 146, 83–97.
Skrutskie, M.F. et al., 2006. The Two Micron All Sky Survey (2MASS). Astron. J. 131, 1163–1183.
Souza, S.P. et al., 2006. POETS: Portable Occultation, Eclipse, and Transit System. Publ. Astron. Soc. Pacific 118, 1550–1557.
Stansberry, J.A., Lunine, J.I., Hubbard, W.B., et al., 1994. Mirages and the nature of Pluto's atmosphere. Icarus 111, 503–513.
Young, L.A., 2013. Pluto's seasons: New predictions for New Horizons. Astrophys. J. 766, L22–L27.
Zacharias, N., Monet, D.G., Levine, S.E., Urban, S.E., Gaume, R., Wycoff, G.L., 2004. The Naval Observatory Merged Astrometric Dataset (NOMAD). In: AAS #405 Abstract #48.15.
Zalucha, A.M., Gulbis, A.A.S., 2012. Comparison of a simple 2-D Pluto general circulation model with stellar occultation light curves and implications for atmospheric circulation. J. Geophys. Res. 117, E05002.
Zangari, A.M., 2013. Investigating Spatial Variation in the Surface and Atmosphere of Pluto through Stellar Occultations and PSF Photometry. PhD Thesis, Department of Earth, Atmospheric, and Planetary Sciences, Massachusetts Institute of Technology, Cambridge, MA.